Comparisons of Channel Emulation Methods for State-of-the-Art Multi-Probe Anechoic Chamber based Millimeter-Wave Over-the-Air Testing

Pei, Huiling; Chen, Xiaoming; Fan, Wei; Zhang, Ming; Zhang, Anxue; Svensson, Tommy

Published in:
2019 IEEE 90th Vehicular Technology Conference (VTC2019-Fall)

DOI (link to publication from Publisher):
10.1109/VTCFall.2019.8891533

Publication date:
2019

Document Version
Accepted author manuscript, peer reviewed version

1) **What is the problem being addressed by the manuscript and why is it important to the Antennas and Propagation community?**

This paper directly compares the emulation performances of the plane wave method and the spherical vector wave method in multi-probe anechoic chamber (MPAC) for over-the-air testing. The direct comparison between the two methods targeting at field synthesis has not yet been implemented previously, and is of great interest since their performances targeting at different directional channels given physical constraints in MPAC could provide instructions on how to use them wisely for future 2.5D and 3D fields emulation. This work is novel and is within the scope of antennas and radio wave propagation, hence is important to the Antennas and Propagation community.

2) **What is the novelty of your work over the existing work?**

The novelties are threefold.

a) The PW and SVW methods on emulating the polarized field in MPAC have been redefined in a uniform manner; the essential reasons for their difference on the probe excitation voltage calculation are analyzed.
b) The performances of the PW and the SVW methods are compared for emulating single path impinging from different direction with different deployments of 2D and 3D probe configurations. The relative errors between emulated and target fields are compared with different settings of probe sphere radius, probe directivity, probe number, probe position and test zone size.
c) Applicable scenarios and instructions on using PW and SVW methods for field emulation in MPAC are discussed.

3) **Provide up to three references, published or under review, (journal papers, conference papers, technical reports, etc.) done by the authors/coauthors that are closest to the present work. Upload them as supporting documents if they are under review or not available in the public domain. Enter "N.A." if it is not applicable.**

- W. Fan, I. Carton, P. Kyosti, and G.F. Pedersen, "Emulating ray-tracing channels in multiprobe anechoic chamber setups for virtual drive testing," *IEEE Trans. Antennas Propag.*, vol. 64, no. 2, pp. 730-739, Feb. 2016.
- W. Fan, X. Carreo, J. Nielsen, J.S. Ashta, G.F. Pedersen, M.B. Knudsen, "Verification of emulated channels in multi-probe based MIMO OTA testing setup," in *Proc. 7th Eur. Conf. Antenna Propag.,* pp. 97-101, Gothenburg, Sweden, Apr. 2013.
- W. Fan, X. Carreno, F. Sun, J. Nielsen, M.B. Knudsen, and G.F. Pedersen, "Emulating spatial characteristics of MIMO channels for OTA testing," *IEEE Trans. Antennas Propag.,* vol. 61, no. 8, pp. 4306-4314, Aug. 2013.

4) **Provide up to three references (journal papers, conference papers, technical reports, etc.) done by other authors that are most important to the present work. Enter "N.A." if it is not applicable.**

- A. Khatun, V.M. Kolmonen, V. Hovinen, D. Parveg, M. Berg, K. Haneda, K.I. Nikoskinen, E.T. Salonen, "Experimental verification of a plane-wave field synthesis technique for MIMO OTA antenna testing," *IEEE Trans. Antennas Propag.*, vol. 64, no. 7, pp. 3141-3150, Jul. 2016.
- P. Kyosti, T. Jamsa, J.P. Nuutinen, "Channel modeling for multiprobe over-the-air MIMO testing," *Int. J. Antennas Propag.,* vol. 2012, no. 615954, 11 pages, Mar. 2012.
- J.T. Toivanen, T.A. Laitinen, V.M. Kolmonen, and P. Vainikainen, "Reproduction of arbitrary multipath environment in laboratory conditions," *IEEE Trans. Instrum. Meas.,* vol. 60, no. 1, pp. 275-281, Jan. 2011.

Comparing Channel Emulation Algorithms by Using Plane Waves and Spherical Vector Waves in Multi-Probe Anechoic Chamber Setups

Yang Miao, Wei Fan, Junichi Takada, Ruisi He, Xuefeng Yin, Mi Yang, José Rodríguez-Piñeiro, Andrés Alayón Glazunov, Wei Wang, Yi Gong

***Abstract*—This paper evaluates the performances of channel emulation algorithms in multi-probe anechoic chamber (MPAC) by using plane wave (PW) and spherical vector wave (SVW) theories. Channel emulation in MPAC enables the over-the-air (OTA) testing of performances of wireless devices under realistic propagation scenarios, through setting excitation voltages of probes and utilizing the polarized radiation patterns, locations and orientations of probe antennas to emulate desired fields in test zone. Accurate emulation of radio wave propagation in target scenario guarantees that the device under test (DUT) be assessed fairly in lab. Dynamic multipath scenario and orthogonal polarization can be emulated by exciting the multiple probes in such a way that the total fields from probes resemble the target impinging field in test zone. The excitation voltages can be either calculated by PW or SVW theories. Despite the fact that PW and SVW are mathematically equal in far field, the different treatment on rotation and translation of waves as well as the different linear equations used in two methods, result in different computed voltages hence different emulated field. The emulation performances of the two methods with different MPAC setup (e.g., test zone size, probe number, probe sphere radius, probe directivity) are investigated. Both scenarios of the 2D field emulation with 2D probe configuration and the 3D (or 2.5D) field emulation with 3D probe configuration are discussed, and instructions on how to use the emulation algorithm wisely are provided.**

***Index Terms*—Over-the-air testing, channel emulation, spherical vector wave, plane wave, multi-probe anechoic chamber, multipath**

I. Introduction

Both quantities and varieties of wireless devices have been experiencing explosive growth and extension. At the same time, the growing demands on more reliable and accessible wireless connections from/to user devices in various physical environments pose higher standards for testing devices before being released to the public. Both the sub-6 GHz and the millimeter wave multiple-input multiple-output (MIMO) systems require better over-the-air (OTA) validation. OTA testing refers to test wireless device in laboratory environment without cables connecting to device, where the minimum performance requirements for single antenna user equipment are defined in terms of transmit power and receiver sensitivity [1]. OTA testing saves time and money for doing on-field measurements where unpredictable problems may occur. Some on-field measurements, e.g. unmanned aerial vehicle networks, can be very difficult to implement and the measured results may not be reproducible due to weather and other issues. On the contrary, testing in lab is more controllable and economic. Moreover, OTA testing does not need to expose the antennas inside devices by destroying the device; instead, it mimics the actual condition when devices are put into use as it is, and mimics the radio waves propagation over the air from base station to user equipment. Based on above, OTA testing is expansively used nowadays.

OTA testing can be implemented in multi-probe anechoic chamber (MPAC) or reverberation chamber. While the former is fading emulator based where arbitrary power angular spectrum (PAS) can be emulated in test zone area [2]–[6], the latter utilizes metallic stirrers in metallic cavity to produce a random variation of field and only uniform PAS can be emulated [7], [8]. OTA testing in MPAC has easier control over the number of multipath, the angular spread, the polarization, as well as the power delay profile and the Doppler effect. For emulating the directional radio channels whose angular dispersion is the crucial characterization, MPAC is the choice. In fact, MPAC OTA testing has been standardized in CTIA [1] and supports standard geometry-based stochastic channel models (GSCM) [9]. In MPAC, the desired spatial and temporal characteristics of intended electromagnetic fields are emulated inside the test zone. The base station signals are generated from the base station emulator and input to the channel emulator. The channel emulator convolves base station signals with propagation channel models and then deliver signals to probes inside chamber. In this process, the Impulse Response (IR) files can be written into channel emulator, and channel emulator will implement the IRs physically. To acquire the IR files, the conversion from radio channels to probe voltages is

Y. Miao is with the Academy for Advanced Interdisciplinary Studies, Southern University of Science and Technology, Shenzhen, China (e-mail: miaoy@sustc.edu.cn). Y. Gong is with the Shenzhen Engineering Laboratory of Intelligent Information Processing for IoT, Southern University of Science and Technology, Shenzhen, China (e-mail: gongy@sustc.edu.cn) W. Fan is with the Dept. of Electronic Engineering, Antennas, Propagation and Millimeter-Wave System (APMS) Group, Aalborg University, Denmark (e-mail: wfa@es.aau.dk). J. Takada is with the Dept. of Trans-disciplinary Science and Engineering, Tokyo Institute of Technology, Tokyo, Japan (email: takada@ide.titech.ac.jp). R. He and M. Yang are from the State Key Lab of Rail Traffic Control and Safety, Beijing Jiaotong University, Beijing, China (e-mail: ruisi.he@bjtu.edu.cn). X. Yin and J. Rodriguez-Pineiro are with the Dept. of Electronics and Information Engineering, Tongji University, Shanghai, China (email: yinxuefeng@tongji.edu.cn, j.rpineiro@tongji.edu.cn). A.A. Glazunov is with the Dept. of Electrical Engineering, University of Twente, Enschede, Netherlands, and he is also with the Dept. of Electrical Engineering in Chalmers University of Technology, Gothenburg, Sweden (email: a.alayonglazunov@utwente.nl). W. Wang is with the School of Information Engineering, Chang'an University, Xi'an, China (email: wei.wang@chd.edu.cn).

necessary, where emulation algorithms are applied. From [10]–[12], the emulation accuracy depends on factors such as the test zone size, the probe configuration (including probe number and positions), the non-ideality of setups, and the emulation algorithms of course.

The emulation algorithms are categorized into the prefaded signal synthesis (PFS) and the plane wave field synthesis (PWS) algorithms [2]–[6]. While the PFS algorithm [2], [6] emulates the target channel cluster-wise and is suitable for stationary channels with specific shape of PAS, the PWS algorithm [2]–[5] is able to reproduce dynamic multipath environment with time-varying PAS and supports orthogonal polarization. PWS algorithm requires phase calibration while PFS algorithm does not. In [13], it is shown that the channel emulated with PWS algorithm is consistent with GSCMs and is more advantageous than PFS algorithm particularly when cluster angular spreads are small. The PWS algorithm can be implemented by using plane wave (PW) [2], [3] or spherical vector wave (SVW) [4], [5] theories. As is known to all, PW is the far field approximation of SVW and is mathematically simple; for the near-field effect (although is not within the scope of this paper), such as the curved wavefront, PW is not applicable and only SVW can be used for proper characterization. In [14], the far-field distance of DUT has been redefined considering the antenna directivity, using the SVW expansion. While the probe directivity is not considered when using PWs realizing PWS algorithm, it is necessary when using SVWs. Moreover, it has been reported that using PW and SVW require different minimum number of probes [4]–[6], [15].

However, to the best of the authors' knowledge, there has been no direct comparison yet between the emulation performances of the PW and the SVW methods even for the basic field synthesis. The comparisons between their emulation capabilities given constraints on the probe number, the probe radius, the probe position and orientation, the test zone size, and the target fields, are extremely attractive; their performances under different circumstances could provide instructions on how to use them wisely for emulating 2D, future 2.5D and 3D fields. This paper is to fill the gap and the contributions are threefold.

1) The PW and SVW methods on emulating the polarized field in MPAC have been redefined in a uniform manner; the essential reasons for their difference on the probe excitation voltage calculation are analyzed.
2) The performances of the PW and the SVW methods are compared for emulating single path impinging from different direction with different deployments of 2D and 3D probe configurations. The relative error between emulated and target fields are compared with different settings of probe sphere radius, probe directivity, probe number, probe position and test zone size.
3) Applicable scenarios and instructions on using PW and SVW methods for field emulation in MPAC are discussed.

The structure for the rest of this paper is as follows. Section II redefines and discusses on the channel emulation algorithms by using PW and SVW methods. Section III compares their performances comprehensively, and Section IV concludes this paper. Throughout the text, the time dependence of radio waves is $e^{-j\omega t}$.

II. Channel Emulation Algorithms

The goal of channel emulation is to generate the desired electromagnetic fields in the test zone so that devices can be tested in emulated fields in anechoic chamber as if it was tested in real-world. In PWS algorithm, a static plane wave with an arbitrary impinging angle can be generated within test area by allocating appropriate complex weights to the probes on the OTA sphere [2]. Either PW or SVW theory can be applied. Referring to [2]–[4], the 3D polarized radio channel emulation is re-defined in this section.

First, the target channel is defined, and we assume it belongs to the GSCM scope. The target channel from n_{T}-th transmit antenna (Tx) to n_{R}-th receive antenna (Rx) is defined by the summation over L paths:

$$\begin{aligned} &h_{n_{\mathrm{R}},n_{\mathrm{T}}}(t,\tau) = \\ &\sum_{l=1}^{L} \begin{bmatrix} F^{\mathrm{R}}_{V,n_{\mathrm{R}}}(\theta_{\mathrm{R},l},\phi_{\mathrm{R},l}) \\ F^{\mathrm{R}}_{H,n_{\mathrm{R}}}(\theta_{\mathrm{R},l},\phi_{\mathrm{R},l}) \end{bmatrix}^{T} \begin{bmatrix} \alpha_{\mathrm{VV},l} & \alpha_{\mathrm{VH},l} \\ \alpha_{\mathrm{HV},l} & \alpha_{\mathrm{HH},l} \end{bmatrix} \begin{bmatrix} F^{\mathrm{T}}_{V,n_{\mathrm{T}}}(\theta_{\mathrm{T},l},\phi_{\mathrm{T},l}) \\ F^{\mathrm{T}}_{H,n_{\mathrm{T}}}(\theta_{\mathrm{T},l},\phi_{\mathrm{T},l}) \end{bmatrix} \\ &\exp(j2\pi\upsilon_l t)\,\delta(\tau-\tau_l) \end{aligned} \tag{1}$$

where F^{R} and F^{T} are the polarimetric radiation patterns of Rx and Tx, respectively. $[\theta_{\mathrm{R}},\phi_{\mathrm{R}}]$ denote the angles of arrival (AoA), $[\theta_{\mathrm{T}},\phi_{\mathrm{T}}]$ denote the angles of departure (AoD), α_{XY} denotes the polarimetric complex gain of path at polarized pair of $XY=\{\mathrm{VV},\mathrm{VH},\mathrm{HV},\mathrm{HH}\}$, υ denotes the Doppler shift, τ denotes the delay, t denotes the time sample or the so-called snapshot, l is the index of path, and L is the total path number. Here the Cartesian coordinate (x,y,z) is convertible to spherical coordinate (r,θ,ϕ), where θ in this paper indicates the co-elevation angle where $\theta=0$ is the north pole and $\theta=\pi$ is the south pole of sphere.

On the other hand, the emulated channel in MPAC to the n_{R}-th Rx is given by:

$$\begin{aligned} &\tilde{h}_{n_{\mathrm{R}}}(t,\tau) \\ &= \sum_{l=1}^{L} \begin{bmatrix} F^{\mathrm{R}}_{V,n_{\mathrm{R}}}(\theta_{\mathrm{R},l},\phi_{\mathrm{R},l}) \\ F^{\mathrm{R}}_{H,n_{\mathrm{R}}}(\theta_{\mathrm{R},l},\phi_{\mathrm{R},l}) \end{bmatrix}^{T} \sum_{p=1}^{P} \boldsymbol{h}_p^{\mathrm{OTA}}(t,\tau)\,\delta(\tau-\tau_l) \end{aligned} \tag{2}$$

where $\boldsymbol{h}_p^{\mathrm{OTA}}$ denotes the emulated channel in test zone contributed from the p-th probe. $\boldsymbol{h}_p^{\mathrm{OTA}}$ contains the effects of 1) the excitation voltages and the gains of the p-th probe antennas, where the excitation voltages are converted from the convolved signals of the output of base station emulator with the propagation channel model by the channel emulator, and 2) the free space propagation from the p-th probe to the test zone. P denotes the total number of probes. $\boldsymbol{h}_p^{\mathrm{OTA}}$ is dealt differently according to PW and SVW theories.

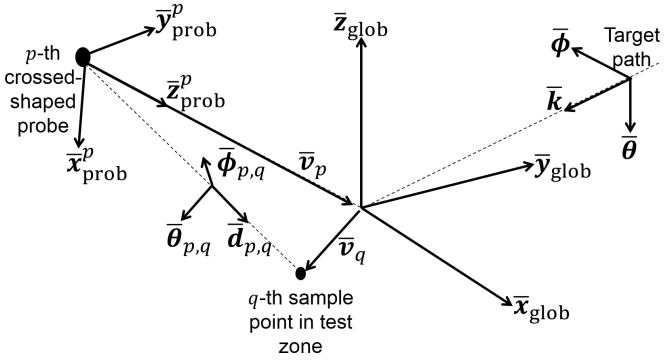

Fig. 1. Coordinate system in MPAC

According to (1) and (2), the target field impinging on Rx in test zone center for the l-th path is characterized as

$$\boldsymbol{E}^{\text{imp}}_{n_{\text{R}},n_{\text{T}},l} = \begin{bmatrix} E^{\text{imp,V}}_{n_{\text{R}},n_{\text{T}},l} \\ E^{\text{imp,H}}_{n_{\text{R}},n_{\text{T}},l} \end{bmatrix} = \begin{bmatrix} \alpha_{\text{VV},l} & \alpha_{\text{VH},l} \\ \alpha_{\text{HV},l} & \alpha_{\text{HH},l} \end{bmatrix} \begin{bmatrix} F^{\text{T}}_{V,n_{\text{T}}}(\theta_{\text{T},l},\phi_{\text{T},l}) \\ F^{\text{T}}_{H,n_{\text{T}}}(\theta_{\text{T},l},\phi_{\text{T},l}) \end{bmatrix} \exp(j2\pi\upsilon_l t) \in \mathbb{C}^{2\times 1}, \tag{3}$$

and it is synthesized by the summation of effects of probes

$$\tilde{\boldsymbol{E}}^{\text{imp}}_{n_{\text{R}},n_{\text{T}},l} = \sum_{p=1}^{P} \boldsymbol{h}^{\text{OTA}}_p(t,\tau). \tag{4}$$

In PWS algorithms, the multipath is synthesized one by one at each snapshot. Note that the probe voltages for field emulation may not need to be re-calculated for each snapshot. As long as the AoA is fixed, the complex weight per antenna is fixed, and a phasor calculated with the Doppler frequency is added to each complex weight.

An ideal plane wave is synthesized by uniform amplitude distribution over the test zone and linear phase front along the propagation direction $\bar{\boldsymbol{k}}$. Setting totally N_q samples within the test zone, the target field of the l-th path at the q-th sample point for one snapshot is given by the spherical vector $\boldsymbol{E}^{\text{imp}}_{n_{\text{R}},n_{\text{T}},l}\exp(j\boldsymbol{k}\cdot\bar{\boldsymbol{v}}_q)$, where $\boldsymbol{k} = \|\boldsymbol{k}\|\cdot\bar{\boldsymbol{k}}$, $\|\boldsymbol{k}\| = 2\pi/\lambda$ is the wavenumber, λ is the wavelength, unit vector is defined by

$$\bar{\boldsymbol{k}} = -\left[\sin(\theta_{\text{R},l})\cos(\phi_{\text{R},l}),\ \sin(\theta_{\text{R},l})\sin(\phi_{\text{R},l}),\ \cos(\theta_{\text{R},l})\right], \tag{5}$$

here "$-$" is added due to the target path is inward propagating. $\bar{\boldsymbol{v}}_q$ is the vector pointing from global coordinate center in test zone to the q-th sample as in Fig. 1.

A. Field Synthesis by Using PW

According to [2], [3], computing the probe excitation voltage by PW method is based on the least square solution of

$$\boldsymbol{E}^{\text{imp}}_{n_{\text{R}},n_{\text{T}},l}\exp(j\boldsymbol{k}\cdot\bar{\boldsymbol{v}}_q) = \sum_{p=1}^{P} \boldsymbol{A}_q^T\boldsymbol{B}_p\cdot\beta_{p,q}\begin{bmatrix} g^{\text{V}}_p \\ g^{\text{H}}_p \\ 0 \end{bmatrix} \tag{6}$$

where the left is the target field and the right is the synthesized field. $\boldsymbol{A}_q^T$ converts the Cartesian vector to the spherical vector in global coordinate $\bar{\boldsymbol{x}}_{\text{glob}}$, $\bar{\boldsymbol{y}}_{\text{glob}}$, $\bar{\boldsymbol{z}}_{\text{glob}}$, and is given by

$$\boldsymbol{A}_q^T = \begin{bmatrix} \sin(\theta_q)\cos(\phi_q) & \cos(\theta_q)\cos(\phi_q) & -\sin(\phi_q) \\ \sin(\theta_q)\sin(\phi_q) & \cos(\theta_q)\sin(\phi_q) & \cos(\phi_q) \\ \cos(\theta_q) & -\sin(\theta_q) & 0 \end{bmatrix}^T. \tag{7}$$

$$\boldsymbol{B}_p = \begin{bmatrix} \cos(\gamma_{z3})\cos(\gamma_{y2})\cos(\gamma_{z1}) - \sin(\gamma_{z3})\sin(\gamma_{z1}), \\ -\cos(\gamma_{z3})\cos(\gamma_{y2})\sin(\gamma_{z1}) - \sin(\gamma_{z3})\cos(\gamma_{z1}), \\ \cos(\gamma_{z3})\sin(\gamma_{y2}); \\ \sin(\gamma_{z3})\cos(\gamma_{y2})\cos(\gamma_{z1}) + \cos(\gamma_{z3})\sin(\gamma_{z1}), \\ -\sin(\gamma_{z3})\cos(\gamma_{y2})\sin(\gamma_{z1}) + \cos(\gamma_{z3})\cos(\gamma_{z1}), \\ \sin(\gamma_{z3})\sin(\gamma_{y2}); \\ -\sin(\gamma_{y2})\cos(\gamma_{z1}), \\ \sin(\gamma_{y2})\sin(\gamma_{z1}), \\ \cos(\gamma_{y2}) \end{bmatrix} \tag{8}$$

is the right-handed transformation matrix from the local probe Cartesian coordinate characterized by $\bar{\boldsymbol{x}}^p_{\text{prob}}$, $\bar{\boldsymbol{y}}^p_{\text{prob}}$ and $\bar{\boldsymbol{z}}^p_{\text{prob}}$ to the global test Cartesian coordinate characterized by $\bar{\boldsymbol{x}}_{\text{glob}}$, $\bar{\boldsymbol{y}}_{\text{glob}}$ and $\bar{\boldsymbol{z}}_{\text{glob}}$. This transformation includes the coordinate rotation which is featured by Euler angle $[\gamma_{z1},\gamma_{y2},\gamma_{z3}]$. From the coordinate featured by $\bar{\boldsymbol{x}}^p_{\text{prob}}$, $\bar{\boldsymbol{y}}^p_{\text{prob}}$ and $\bar{\boldsymbol{z}}^p_{\text{prob}}$, rotate about z^p_{prob} axis with angle γ_{z1} then we get coordinate $\left(x'^p_{\text{prob}}, y'^p_{\text{prob}}, z'^p_{\text{prob}}\right)$; rotate about y'^p_{prob} axis with angle γ_{y2} then we get coordinate $\left(x''^p_{\text{prob}}, y''^p_{\text{prob}}, z''^p_{\text{prob}}\right)$; rotate about z''^p_{prob} axis with angle γ_{z3} then we get the test zone coordinate featured by $\bar{\boldsymbol{x}}_{\text{glob}}$, $\bar{\boldsymbol{y}}_{\text{glob}}$ and $\bar{\boldsymbol{z}}_{\text{glob}}$. $\beta_{p,q}$ is the propagation coefficient from the p-th probe to the q-th sample point, given by

$$\beta_{p,q} = \frac{\lambda}{4\pi\|\bar{\boldsymbol{v}}_p + \bar{\boldsymbol{v}}_q\|}\exp(j\|\boldsymbol{k}\|\cdot\|\bar{\boldsymbol{v}}_p + \bar{\boldsymbol{v}}_q\|). \tag{9}$$

g^{V}_p and g^{H}_p are the excitation voltages assigned for p-th probe antennas. Note that (6) is defined based on the coordinate system in Fig. 1, and different coordinate system may result in slightly different form in (6).

Here, the radiation patterns of probes are ignored, due to the most important assumption (or simplification) that the probe radiation patterns are constant on the edge or within the test zone. Given that the test zone sphere radius is normally set to be much smaller than the probe sphere radius, the variations of the radiation patterns of probes over small angles are ignored.

B. Field Synthesis by Using SVW

According to [4], [5], computing the probe excitation voltage by SVW method is based on the least square solution of

$$\boldsymbol{Q} = \sum_{p=1}^{P} \begin{bmatrix} U^{p,V}_1 & U^{p,H}_1 \\ \vdots & \\ U^{p,V}_{j'} & U^{p,H}_{j'} \\ \vdots & \\ U^{p,V}_J & U^{p,H}_J \end{bmatrix} \begin{bmatrix} g^{\text{V}}_p \\ g^{\text{H}}_p \end{bmatrix}, \tag{10}$$

i.e. $\boldsymbol{Q} = \boldsymbol{U}\boldsymbol{g}$ where $\boldsymbol{Q} \in \mathbb{C}^{J\times 1}$ represents the target field in SVW domain, $\boldsymbol{U} \in \mathbb{C}^{J\times 2P}$, $\boldsymbol{g} \in \mathbb{C}^{2P\times 1}$, $\boldsymbol{U}\boldsymbol{g}$ represents the

synthesized field in SVW domain, $j' = 1, 2, \ldots, J$ denotes the SVW mode index, and J denotes the total mode number.

On one hand, the target impinging fields to Rx in test zone can be represented by the SVW expansion in the source-free region [16]

$$\begin{aligned} &\boldsymbol{E}^{\mathrm{imp}}_{n_{\mathrm{R}},n_{\mathrm{T}},l} \exp\left(j\boldsymbol{k}\cdot\bar{\boldsymbol{v}}_q\right) = \\ &k\sqrt{\eta}\sum_{s=1}^{2}\sum_{n=1}^{N}\sum_{m=-n}^{n} Q_{smn}\boldsymbol{F}^{(1)}_{smn}\left(r_q,\theta_q,\phi_q\right). \end{aligned} \tag{11}$$

$\boldsymbol{F}^{(1)}_{smn}$ is the power normalized spherical wave function (SWF) for the standing wave and is a solution of the homogeneous vector Helmholtz equation in the spherical coordinates. Q_{smn} is the spherical wave coefficient (SWC). $s = 1$ and $s = 2$ denote the TE and TM modes, respectively, $n = 1, 2, 3, \ldots$ are mode indices for θ direction, and $m = -n, -n+1, \ldots, n-1, n$ are for ϕ direction. This triple indices smn is equivalent to the single index $j' = 2\{n(n+1) + m - 1\} + s$. N is the finite truncation number and depends on the electric size of antenna. Assuming r_0^{t} and r_0^{r} are the radii of the minimum spheres enclosing Tx and Rx, respectively, N can be set as $\lfloor kr_0 \rfloor + 10$ where $r_0 = \max\left(r_0^{\mathrm{t}}, r_0^{\mathrm{r}}\right)$. The total modes number is thus determined to be $J = 2N(N+2)$. This truncation is one of the most important properties of the SVW expansion. $k = \|\boldsymbol{k}\|$, and $\eta \simeq 120\pi$ is the wave impedance. Coefficient $k\sqrt{\eta}$ is to ensure the normalization condition that unit SWC corresponds to 1 $\mathrm{W}^{\frac{1}{2}}$. (r_q, θ_q, ϕ_q) is the global spherical coordinate featured by $\bar{\boldsymbol{x}}_{\mathrm{glob}}$, $\bar{\boldsymbol{y}}_{\mathrm{glob}}$, $\bar{\boldsymbol{z}}_{\mathrm{glob}}$ in Fig. 1. (11) is essentially **the SVW expansion of plane wave, and is only valid when** $r_q < R \approx N/k$ [16]. The solution of SWC to the expansion in (11) is

$$Q_{smn} = \frac{1}{k\sqrt{\eta}}(-1)^m\sqrt{4\pi}j\boldsymbol{E}^{\mathrm{imp}}_{n_{\mathrm{R}},n_{\mathrm{T}},l}\cdot\boldsymbol{K}_{s,-m,n}\left(\theta_{\mathrm{R},l},\phi_{\mathrm{R},l}\right) \tag{12}$$

where $\boldsymbol{K}_{smn}$ is the far-field pattern SWF defined in [16] and can be found in Appendix A.

On the other hand, the synthesized polarized fields in the test zone are the summation of the radiated, translated and rotated SVWs from probes [16]:

$$\begin{aligned} &\tilde{\boldsymbol{E}}^{\mathrm{imp}}_{n_{\mathrm{R}},n_{\mathrm{T}},l} \exp\left(j\boldsymbol{k}\cdot\bar{\boldsymbol{v}}_q\right) \\ &= k\sqrt{\eta}\sum_{p=1}^{P}\sum_{j'=1}^{J}\boldsymbol{U}^p_{smn}\begin{bmatrix} g_p^{\mathrm{V}} \\ g_p^{\mathrm{H}}\end{bmatrix}\boldsymbol{F}^{(1)}_{smn}\left(r_q,\theta_q,\phi_q\right) \end{aligned} \tag{13}$$

$$\begin{aligned} \boldsymbol{U}^p_{smn} = &\sum_{\sigma=1}^{2}\sum_{\upsilon=1}^{N'}\sum_{\mu=-\upsilon}^{\upsilon}\sum_{\mu_1=-\min(\upsilon,n)}^{\min(\upsilon,n)} e^{j\mu\phi_0}d^{\upsilon}_{\mu_1\mu}\left(\theta_0\right)e^{j\mu_1\chi_0} \\ &C^{\sigma\upsilon(3)}_{s\mu_1 n}\left(k\|\bar{\boldsymbol{v}}_p\|\right)e^{j\mu_1\phi_0'}d^{n}_{m\mu_1}\left(\theta_0'\right)e^{jm\chi_0'}\begin{bmatrix} T^{p,\mathrm{V}}_{\sigma\mu\upsilon} \\ T^{p,\mathrm{H}}_{\sigma\mu\upsilon}\end{bmatrix}^T \end{aligned} \tag{14}$$

where $\boldsymbol{U}^p_{smn}$ is the probe SWC taking into account the probe location, orientation and polarization. $\sigma\mu\upsilon$ is used to indicate the SVW modes in the local coordinate of each probe. $T^p_{\sigma\mu\upsilon}$ is the normalized SWC of the p-th probe at its local coordinate, and can be calculated from its radiation pattern. $C^{\sigma\upsilon(3)}_{s\mu_1 n}$ is the translation coefficient of SWF where the translation distance is assumed to be larger than the electric size of probe. The SVW rotation coefficients $d^{\upsilon}_{\mu_1\mu}$ and $d^{n}_{m\mu_1}$ are real functions, $e^{j\mu_1\phi_0'}d^{n}_{m\mu_1}\left(\theta_0'\right)e^{jm\chi_0'}$ denotes the rotation of SWF about Euler angle $[\phi_0', \theta_0', \chi_0']$, and $e^{j\mu\phi_0}d^{\upsilon}_{\mu_1\mu}\left(\theta_0\right)e^{j\mu_1\chi_0}$ denotes the rotation about $[\phi_0, \theta_0, \chi_0]$. The first and the third Euler angles denote the rotation angle about z-axis, and the second denotes the rotation angle about y-axis. We follow explicitly the formulas in Hansen's book [16], where the transformation of the SWFs in the probe coordinate to that in the global coordinate is decomposed into three steps, i.e. rotation, translation and rotation again; please see Appendix B for detailed derivation. Since the translation formula provided by Hansen is only for the translation along the **positive z-axis**, following probe coordinate in Fig. 1, $[\phi_0, \theta_0, \chi_0]$ should be set to $[0, 0, 0]$, and $[\phi_0', \theta_0', \chi_0']$ to $[\gamma_{z_1}, \gamma_{y_2}, \gamma_{z3}]$, hence (14) becomes

$$\begin{aligned} \boldsymbol{U}^p_{smn} = &\sum_{\sigma=1}^{2}\sum_{\upsilon=1}^{N'}\sum_{\mu=-\min(\upsilon,n)}^{\min(\upsilon,n)} \\ &C^{\sigma\upsilon(3)}_{s\mu n}\left(k\|\bar{\boldsymbol{v}}_p\|\right)e^{j\mu\gamma_{z_1}}d^{n}_{m\mu}\left(\gamma_{y_2}\right)e^{jm\gamma_{z_3}}\begin{bmatrix} T^{p,\mathrm{V}}_{\sigma\mu\upsilon} \\ T^{p,\mathrm{H}}_{\sigma\mu\upsilon}\end{bmatrix}^T. \end{aligned} \tag{15}$$

C. Applicability

Applications of PW and SVW methods are similar in:

1) both require the amplitude and phase calibrations of probes;
2) both support the polarized and dynamic channel models.

Distinctions of the applicability of PW and SVW methods are as follows.

1) The PW method does not require probe radiation pattern, and it assumes that the probes are point sources. The point source assumption can be satisfied by setting the probe sphere radius to be much larger than the test zone radius so that the radiation pattern variation over a small angle can be ignored. SVW method requires probe radiation patterns and accurate placement of probes, since spherical wave expansion is sensitive to the offset of probes.
2) Leave alone the GSCM for the moment, PW method assumes that the target radio channel is measured/modeled when the interacting objects are far away from Rx, and the surfaces of interacting objects are smooth comparing to wavelength, so that the radio channel can be modeled accurately using distinct plane waves. SVW method does not put assumption on target channel, and the near-field effect, the interaction of radio waves with objects having complex shapes or rough surfaces can be modeled; in such scenario, we simply need to replace the target field in (11), (13) to the antenna de-embedded propagation channel [17], [18].
3) Back to the GSCM emulation, the solution of probe excitation voltage by PW method in (6) and that by SVW method in (10) are based on different linear problems. The former is based on the linear problem of fields, and the latter is based on the linear problem of the complex weights of orthogonal SVW modes. In PW method, the

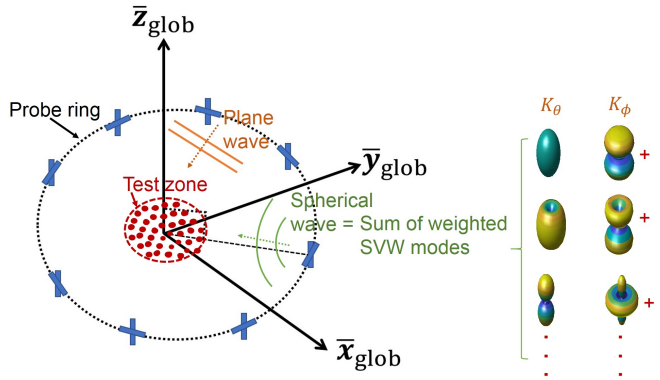

Fig. 2. Schematic diagram for 2D probe configuration as well as PW and SVW, where $\boldsymbol{K}$ denotes the spherical wave functions and its definition can be found in Appendix A

condition of solving the linear problem depends on the sampling field, and the best way is to sample on the test zone sphere surface. In SVW method, the introduction of higher order evanescent modes causes ill-conditioned linear problem in (10), but results in more accurate synthesize of fields in (11), (13). Since the priority is to estimate probe voltages accurately, a proper truncation number needs to be applied in SVW methods.

III. Performance Comparison

In this section, the performances of PW and SVW methods on emulating the channel belonging to GSCM scope are compared. In actual process, the complex voltages emulating each single path for each cluster at each snapshot are consecutively input to probes to "replay" the radio propagation channel in MPAC. Therefore, the emulation accuracy of PW and SVW methods targeting for single path impinging from different direction is the essential issue. First, the 2D field emulation using 2D probe configuration is discussed. Then, the 2.5D or 3D field emulation using 3D probe configuration is discussed. Here the 2D field indicates that each single path impinges on test zone from the direction whose co-elevation AoA is $\frac{\pi}{2}$, i.e. on equator plane; the 2.5D field [19] indicates that each single path impinges from the direction whose co-elevation AoA is $\frac{\pi}{2}\pm\Delta\theta$, i.e. concentrated around equator; the 3D field indicates that each single path may impinge from any direction.

A. Emulation with 2D probe configuration

To start with, 2D probe configuration is adopted to emulate target 2D field. As is shown in Fig. 2, the 2D configuration indicates that probes are deployed on the equator of probe sphere, or the so-called probe ring. The emulation performances by using PW and SVW methods are compared with different settings of MPAC factors (i.e. different type of probe antennas, different probe number or probe deployment density in other words, different probe ring radius), different test area radius, and different target single path. The algorithm emulation accuracy is evaluated according to the relative error δ between the emulated field $\tilde{\boldsymbol{E}}$ and the target field $\boldsymbol{E}$

$$\begin{aligned}\delta_{\text{PW}} &= 10\log_{10}\frac{\sum_q\left|\tilde{\boldsymbol{E}}_{\text{PW}}-\boldsymbol{E}\right|^2}{\sum_q|\boldsymbol{E}|^2},\\ \delta_{\text{SVW}} &= 10\log_{10}\frac{\sum_q\left|\tilde{\boldsymbol{E}}_{\text{SVW}}-\boldsymbol{E}\right|^2}{\sum_q|\boldsymbol{E}|^2}.\end{aligned} \tag{16}$$

where $\tilde{\boldsymbol{E}}_{\text{PW}}$ and $\tilde{\boldsymbol{E}}_{\text{SVW}}$ denote the emulated fields, δ_{PW} and δ_{SVW} denote the relative errors by PW and SVW methods, respectively. q is defined in the same way as in Fig. 1 and in Section II, i.e., the index of samples in test zone. In the performance evaluation process, the probe voltages are estimated from the target field samples in test zone by solving (6) and (10), and the emulated fields are obtained from the estimated voltages following the right side of equations (6) and (13), respectively.

Particularly, the probe radiation patterns are required in the SVW method to calculate the normalized SWC $\boldsymbol{T}$ in (14), (15). Each probe is composed of two cross-shaped antennas to implement the two orthogonal polarizations of fields, and the two antennas are independently fed and absorber nested. The radius of the minimum enclosing sphere of probe antennas is denoted as r_0, and the minimum required truncation number N' is $\lfloor kr_0\rfloor$ where the corresponding $2\lfloor kr_0\rfloor(\lfloor kr_0\rfloor+2)$ modes are the so-called major modes [16], [17], [20]. Higher order modes in addition to the major modes are evanescent, and could cause ill-condition issues in (10) hence can be ignored. On the other hand, the truncation number N describing the target impinging field should at least satisfy $N \geqslant \lfloor kR_{\text{test}}\rfloor$ that relates to the test zone radius R_{test}. According to [15], [16], the rule of thumb for the minimum required number of probes (note that one probe has two antennas) is $2P \geqslant 2N+1$ in case of 2D probe configuration. With the increase of frequency, i.e. with the increase of wavenumber k, the required number of probes also increases for the same desired test zone size. In addition, as probe radiation patterns are required in SVW method but not in PW method, one may wonder whether the radiation pattern or antenna directivity matters; to this end, the cross-shaped Vivaldi antennas (directional) [21] as well as the cross-shaped Dipole antennas (omnidirection) are used as probe antennas for emulation performance comparison. Note that the electrical sizes of the two types of antennas are set to be equal for fair comparison, and the diameter of the minimum enclosing sphere of the cross-shaped antennas is 0.3 m in the numerical examples. Moreover, their radiation patterns used in this paper are obtained from the MATLAB antenna toolbox.

1) Emulation performance vs. Probe number: Assume that the operating frequency is 1 GHz, the test zone radius R_{test} is 0.35λ, the probe ring radius R_{probe} is 2 m ($\approx 19R_{\text{test}}$), and the probe number P ranges from 2 (probe angular separation 180°) to 16 (probe angular separation 22.5°). Supposing the target field is a single path with circular polarization impinging from $[\theta_{\text{R}},\phi_{\text{R}}] = [90°, 0°]$ (denoted as path A) or from $[\theta_{\text{R}},\phi_{\text{R}}] = [90°, 22.5°]$ (denoted as path B), the relative errors between the emulated and the target fields over the number of

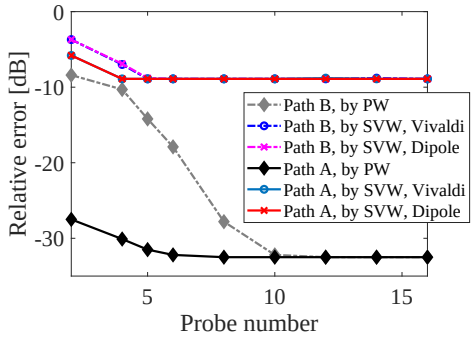

Fig. 3. Relative errors between emulated and target fields, by using PW and SVW (with cross-shaped Vivaldi antennas as probe, or with cross-shaped Dipole antennas as probe) methods, with different settings of probe number

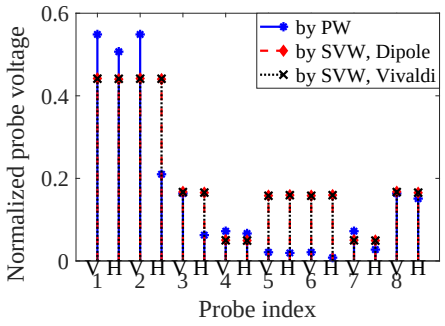

Fig. 4. Amplitudes of normalized probe voltages emulating path B by PW and SVW methods when probe number is set to 8

probes are shown in Fig. 3. It can be observed that with the increase of probe number, the emulation error converges. By using PW method, the emulation error converges to -32 dB with probe number equal to or larger than 6 for path A and 10 for path B. By using SVW method, first, the performance when probe is composed of cross-shaped Vivaldi antennas and that when Dipole antennas have no obvious difference. This is within expectation, because that the relative structure of $\boldsymbol{U}^p$ for all probes does not vary with the change of $\boldsymbol{T}$ in (14), (15), as long as the two types of antennas have the same electrical size therefore the same number of major SVW modes. Second, the emulation error converges to -9 dB with probe number being no less than 4 for path A, and no less than 5 for path B. Comparing the performances of the two algorithms, it can be found that less probe number is required by using SVW method for a converged emulation accuracy. However, to emulate the 2D field impinging from equator plane, SVW method does not perform as good as PW method, which is most likely due to the uninvolved elevation direction mode index n, υ in (14), (15) and the resulting ill-condition of $\boldsymbol{U}$. For visualization purpose, the probe voltages emulating path B by two methods with 8 probes are shown in Fig. 4, and the resulting emulated fields in equator plane are shown in Fig. 5. Interestingly, in Fig. 4, the computed voltages are the same in amplitude for two ports of each probe when using SVW method, which is ideal and could be the result of using the SVW modes of polarized radiation patterns as well as the

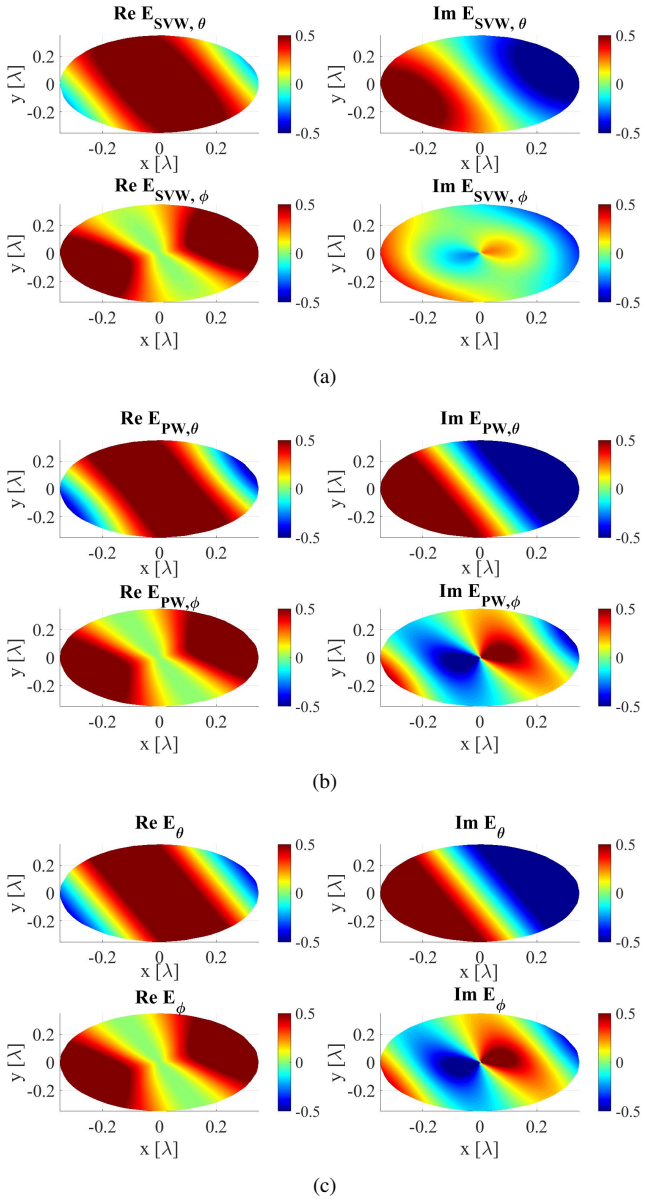

Fig. 5. Patterns on equator plane within test zone: (a) the emulated field by SVW method with cross-shaped Dipole antennas as probe when probe number is set to 8 (b) the emulated field by PW method when probe number is set to 8 (c) the target field of path B

rotation and translation functions of SVWs in (14), (15). In Fig. 5, the real and imaginary parts of the emulated fields are shown together with the reference fields. Obvious discrepancy between the imaginary part of the emulated field by SVW method and that of the reference can be observed.

2) Emulation performance vs. Probe ring radius: Assume that the frequency is 1 GHz, the test zone radius is 0.35λ, and the probe number is 8. Since the performance of SVW method was found to not vary with the change of directivity of probe antennas once the antenna electrical size keeps the same (so as the excited major SVW modes number), the cross-shaped Vivaldi antennas are used as probe from now on. With different probe ring radius R_{probe} ranging from 0.15 m ($\approx 1.5R_{\text{test}}$) to 2.5 m ($\approx 25R_{\text{test}}$), the emulation accuracies by PW and

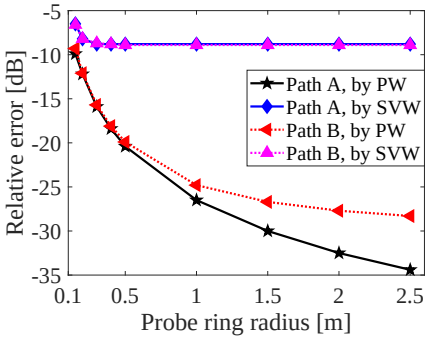

Fig. 6. Relative errors between emulated and target fields, by using PW and SVW (with cross-shaped Vivaldi antennas as probe) methods, with different settings of probe ring radius

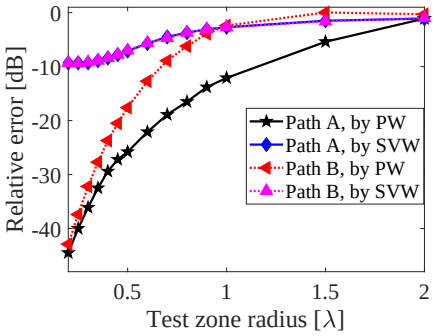

Fig. 7. Relative errors between emulated and target fields, by using PW and SVW (with cross-shaped Vivaldi antennas as probe) methods, with different settings of test zone radius

SVW methods are shown in Fig. 6. It can be observed that the emulation performance using SVW method is not influenced by the variation of probe ring radius when it is set to be larger than $2R_{\text{test}}$, and the emulation accuracy using PW method tends to be higher when probe ring radius increases. In PW method, since each probe is treated as a point source, the further the distance between the probe ring and the test zone, the better; it is also found that the emulation error tends to converge with the increase of probe ring radius.

3) Emulation performance vs. Test zone radius: Assume that the frequency is 1 GHz, the probe number is 8, the probe ring radius is 2 m, and each probe is composed of cross-shaped Vivaldi antennas. With different test area radius ranging from 0.2λ to 2λ, the emulation accuracy by PW and SVW methods are shown in Fig. 7. Comparing the two algorithms, both tend to have larger emulation errors with the increase of test zone size. The speed of emulation error increment when using PW method is larger than that when using SVW method. In SVW method, the change of test zone radius from 0.2λ to 2λ results in the change of the minimum required probe number from $\left(2\lfloor\frac{2\pi}{\lambda}\cdot 0.2\lambda\rfloor+1\right)/2\approx 2$ to $\left(2\lfloor\frac{2\pi}{\lambda}\cdot 2\lambda\rfloor+1\right)/2\approx 13$. With probe number being set to 8, the behavior of the emulation accuracy of SVW algorithm with the change of test zone radius in Fig. 7 can be expected. It is also worth mentioning that the test zone size should not be set to be too large to avoid that the emulation accuracy is too bad.

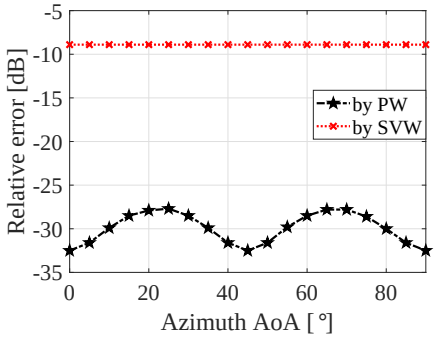

Fig. 8. Relative errors between emulated and target fields, by using PW and SVW (with cross-shaped Vivaldi antennas as probe) methods, for different azimuth AoA of target single path

4) Emulation performance vs. Azimuth AoA of target path: Assume that the frequency is 1 GHz, the probe ring radius is 2 m, the probe number is 8, each probe is composed of two cross-shaped Vivaldi antennas, and the test zone radius is 0.35λ. Here the emulation performances of PW and SVW methods are compared for various azimuth AoA ϕ_{R} of target single path. Suppose that ϕ_{R} is valued from 0° to 90°, the relative errors by using PW and SVW methods are shown in Fig. 8. The target-dependent performance of PW method has been observed. PW method works excellently when the direction of target impinging path coincides with the probe position on probe sphere, and the relative larger emulation error occurs when the direction of target impinging path aligns in between two probes. As to the SVW method, the performance does not vary with the target field, rather it is influenced by the probe configuration and the truncation number of SVW expansion, as was analyzed previously.

B. Emulation with 3D probe configuration

Here, the 3D probe configuration is adopted to emulated the 2.5D or the 3D field. As is shown in Fig. 9, the 3D configuration indicates that probes are deployed not only on the equator of probe sphere, but also on the north and south hemispheres. The latitudes of the probes except for those on equator are denoted by θ_{up} and θ_{down}. The principle of the 3D probe deployment considered in this paper is to guarantee that **the distances between probes are approximately equal**, therefore

$$\begin{gathered}(G+1)\,\theta_{\text{up},1}=\frac{\pi}{2},\ \theta_{\text{up},g}=g\theta_{\text{up},1},\ \theta_{\text{up},g}+\theta_{\text{down},g}=\pi,\\ R_{\text{probe}}\frac{\pi}{2}\frac{1}{G+1}=R_{\text{probe}}\Delta\phi_{\theta=\frac{\pi}{2}},\\ R_{\text{probe}}\sin\theta_{\text{up},g}\Delta\phi_g=R_{\text{probe}}\Delta\phi_{\theta=\frac{\pi}{2}}\end{gathered}\tag{17}$$

where $g=1,\ldots,G$ is the index and G is the total number of probe altitude in one hemisphere excluding the equator, $\Delta\phi_g$ indicates the azimuth angular separation of probes at the gth latitude, and $\Delta\phi_{\theta=\frac{\pi}{2}}$ indicates the azimuth angular separation of probes on equator. Therefore, once G is determined, the 3D probe configuration with equal-distance is fixed. For instance,

TABLE I
EXAMPLES OF 3D PROBE CONFIGURATION WITH APPROXIMATELY EQUAL-DISTANCE

No. 1	θ_{probe}	45° ($\theta_{\text{up},1}$), 135° ($\theta_{\text{down},1}$)	90°	
$G=1$	ϕ_{probe}	0°, 60°, 120°, 180°, 240°, 300°	0°, 45°, 90°, 135°, 180°, 225°, 270°, 315°	
No. 2	θ_{probe}	30° ($\theta_{\text{up},1}$), 150° ($\theta_{\text{down},1}$)	60° ($\theta_{\text{up},2}$), 120° ($\theta_{\text{down},2}$)	90°
$G=2$	ϕ_{probe}	0°, 60°, 120°, 180°, 240°, 300°	0°, 36°, 72°, 108°, 144°, 180°, 216°, 252°, 288°, 324°	0°, 30°, 60°, 90°, 120°, 150°, 180°, 210°, 240°, 270°, 300°, 330°
No. 3	θ_{probe}	30° ($\theta_{\text{up},1}$), 150° ($\theta_{\text{down},1}$)	90°	
	ϕ_{probe}	0°, 90°, 180°, 270°	0°, 45°, 90°, 135°, 180°, 225°, 270°, 315°	

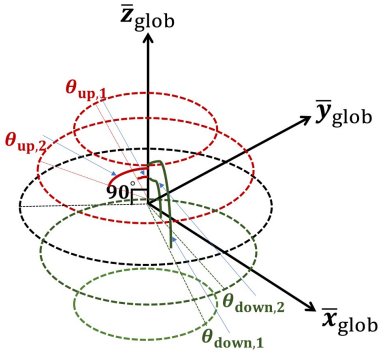

Fig. 9. Schematic diagram for considered 3D probe configuration

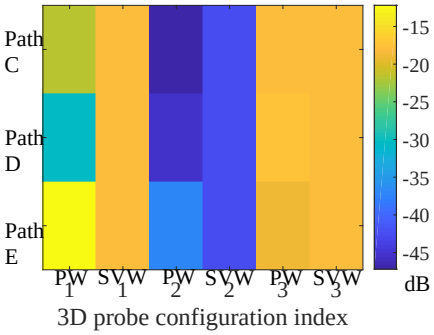

Fig. 10. Relative errors between emulated and target fields, by using PW and SVW (with cross-shaped Vivaldi antennas as probe) methods, with different settings of 3D probe configuration and numbers

when setting $G=1$ and $G=2$, the probe configurations are shown in Table I.

1) Emulation performance vs. Probe configuration: Assume that the operating frequency f is 1 GHz, the test zone radius R_{test} is 0.35λ, and the probe sphere radius R_{probe} is 2 m. The probe configuration follows Table I. The probe number P is 20 and the distance between probes is approximately $R_{\text{probe}}\frac{\pi}{4}$ when $G=1$; $P=44$ and the probe distance is about $R_{\text{probe}}\frac{\pi}{6}$ when $G=2$. The configuration No. 3 does not hold for probes being equidistant (probe distance in elevation domain $R_{\text{probe}}\frac{\pi}{3}$ is larger than that in azimuth domain $R_{\text{probe}}\frac{\pi}{4}$) and is used for comparison purpose. The target field is supposed to be a single path with circular polarization impinging from $[\theta_{\text{R}},\phi_{\text{R}}]=[75°,15°]$ (denoted as path C), or from $[\theta_{\text{R}},\phi_{\text{R}}]=[45°,15°]$ (denoted as path D), or from $[\theta_{\text{R}},\phi_{\text{R}}]=[15°,15°]$ (denoted as path E). The resulting emulation relative errors by using PW and SVW methods with different 3D probe configurations are shown in Fig. 10. Note that in Section III A, the emulation accuracy is analyzed on the 2D azimuth equator plane; from here, the emulation accuracy will be analyzed on the 3D test zone sphere. In addition, same as in the 2D case, it is also found that the SVW performance does not depend on the antenna type used, hence the results using Vivaldi antennas as probe components are presented. As is observed from figure, the SVW method performs stably regardless of the target path while the PW method performs depending on the target path. Both methods perform the best with probe configuration No. 2, which is within expectation. It can be explained according to the SVW theory [16], [17], where the number of the fully excited SVW modes is in proportional to the richness of positions of deployed antennas on sphere. With larger number of fully excited SVW modes, a proper condition number of $\boldsymbol{U}$ with larger dimension is guaranteed. In addition, SVW method does not perform significantly different with configuration No. 1 and No. 3, which probably due to the similar condition of the excitation of the elevation SVW mode indices. By PW method, similar as in 2D case, the emulation error is the least when the direction of the target impinging path coincides with the probe location on probe sphere.

2) Emulation performance vs. Probe sphere radius: Assume that the frequency is 1 GHz, the test zone radius is 0.35λ, the probe configuration is No. 1 in Table I, and the probe antenna type is Vivaldi antenna. The emulation performances of PW and SVW methods are analyzed with the change of probe sphere radius, where R_{probe} ranges from 0.15 m to 2.5 m. The resulting emulation accuracies are shown in Fig. 11. Similarly as in 2D case, when using SVW method, the emulation performance is not influenced by the variation on probe sphere radius; when using PW method, different from the 2D case, the emulation performance may be influenced by the variations on probe sphere radius, and the influence is target dependent and is concentrated when the probe sphere radius is smaller than 0.5 m ($\approx 5R_{\text{test}}$).

3) Emulation performance vs. Test zone radius: Assume that the frequency is 1 GHz, the probe configuration is No. 1 in Table I, the probe antenna type is Vivaldi antenna, and the probe sphere radius is 2 m. With different test zone radius ranging from 0.2λ to 2λ, the emulation accuracies by using PW and SVW methods are shown in Fig. 12. Comparing between two methods, the emulation accuracy decreases with the increase of test zone radius. To keep the emulation error no larger than -10 dB, it had better to keep the test zone radius no larger than 0.5λ regardless of the target path if using SVW method; if using PW method, it had better to keep the test

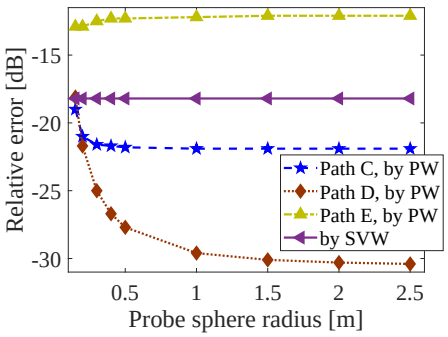

Fig. 11. Relative errors between emulated and target fields, by using PW and SVW (with cross-shaped Vivaldi antennas as probe) methods, with different settings of probe sphere radius

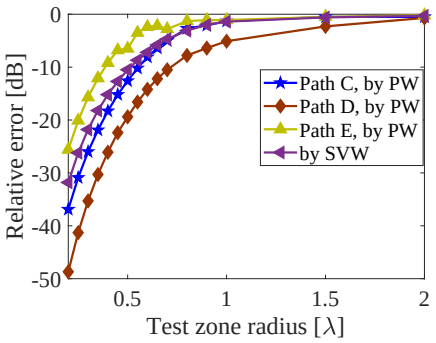

Fig. 12. Relative errors between emulated and target fields, by using PW and SVW (with cross-shaped Vivaldi antennas as probe) methods, with different settings of test zone radius

zone radius less than 0.55λ, 0.7λ, 0.4λ to emulate path C, D, E, respectively with errors less than -10 dB.

4) Emulation performance vs. AoA of target path: Following the previous part, the target dependent performance of PW method may need to be analyzed with different elevation and azimuth AoA of target path. Assume that the frequency is 1 GHz, the probe configuration is No. 1 in Table I, the probe sphere radius is 2 m, each probe is composed of cross-shaped Vivaldi antennas, and the test zone radius is set to 0.5λ. The target path is assumed to impinge on test zone with AoA covering one eighth sphere, i.e. θ_{R} ranges from 0° to 90° while ϕ_{R} ranges from 0° to 90°. While the emulation errors using SVW method stay at the level of -10.5 dB regardless of the target, those by using PW method are shown in Fig. 13. It can be observed that for paths with elevation AoA being 15°, the emulation errors are larger than -10 dB. It is within expectation that, as probes are treated as point sources in PW method, when the direction of target impinging field does not coincide with probes deployed on sphere, or when there is no probes deployed near the target direction, the emulation accuracy drops. In this example, the probes are deployed at elevation levels of 45°, 90°, 135°; the direction with elevation AoA being 15° is not in between the probe elevation levels, and is far away from probes at elevation level 45°, therefore, the worst emulation accuracy when using PW method can be expected.

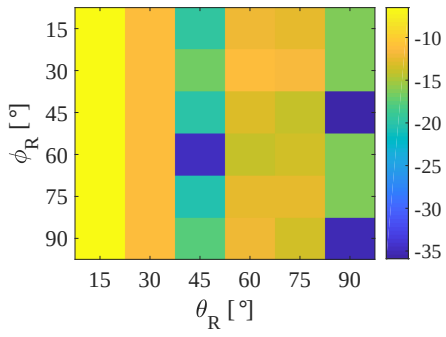

Fig. 13. Relative errors between emulated and target fields, by using PW method, with different target path

C. Discussion

From above, the PW method performs dependently on the AoA of target field, while the SVW method performs regardless of neither the AoA of target field nor the probe antennas' type once the probe configuration is fixed. With 2D probe configuration, PW method achieves higher emulation accuracy than SVW method, owing to the ill-condition of $\boldsymbol{U}$ in (10) caused by the non-involvement of the elevation mode index in SVW method when calculating the probe voltages. With 3D probe configuration, SVW method performs more stably than PW method, since the probe voltages are calculated through the matrix inversion of fully excited modes, and the condition of the inversion of the orthogonal SVW modes is fixed once the probe configuration is determined.

IV. Conclusion

This paper targets at the plane wave synthesis emulation algorithms in multi-probe anechoic chamber for the purpose of the over-the-air testing. This paper re-defined the emulation algorithm by using plane wave method and that by using spherical vector waves method in a uniform manner, and compared their performances on emulating different single path, given different probe configuration and test zone size.

As the goal in field emulation is to obtain the excitation voltages for the cross-shaped probe antennas deployed on sphere, the discrepancies of the PW and the SVW emulation algorithms in calculating the voltages were analyzed. Two methods depend on different linear equations: 1) the equation in PW method is based on the sampling fields, and the condition for solution depends on the coordinate rotation matrices and the free-space translation function, assuming the probes are point sources and the small angular variations of probe antennas' radiation patterns in test zone are ignored; 2) the equation in SVW method is based on the coefficients of orthogonal spherical vector wave modes, and the condition depends on the rotation and translation of spherical vector waves as well as the transmission spherical wave coefficients of probe antennas.

Numerical examples were presented to compare the performances of PW and SVW methods, giving different probe configuration, probe number, probe sphere radius, test zone

radius, and different target path impinging on test zone from different direction.

- With 2D probe configuration, PW method is preferable to SVW method in emulating the 2D field; it can be explained by SVW theory that the SVW expansion of 2D field does not involve the elevation mode index hence results in ill-condition in linear equation when computing probe voltages. Besides, larger probe number is required in PW method for a converged emulation error, and the probe ring radius affect slightly the emulation performance of PW method once it is in the far field of test zone. Both methods perform less accurately with the increase of test zone size; with 2D probe configuration, the influence of test zone size on PW method is larger than that on SVW method. Moreover, PW method is found to be target dependent.
- With 3D probe configuration, SVW method is preferable to PW method in emulating the 2.5D or 3D field, since the former performs stably regardless of the target path and the probe antennas' type once the probe configuration and antennas' electrical sizes are fixed. PW method performs excellently when emulating certain path directions, but not those whose impinging AoA directions do not align in between or near deployed probes. The emulation accuracies of both methods increase with the increase of the richness of probe positions (especially the elevation deployment), which can be explained by SVW theories as to the fully excitation of spherical wave modes. With 3D probe configuration, both methods seem to be not influenced by probe sphere radius when it is larger than five times the test zone size. To ensure that the emulation error of 2.5D or 3D field is less than certain level, different maximum test zone sphere radius may be required if using PW method because its performance depends on the relative positions of the target impinging direction comparing to the probes deployed.

APPENDIX

A. Far-Field Pattern Spherical Wave Functions

$$\begin{aligned}\boldsymbol{K}_{1mn}(\theta,\phi) = &\sqrt{\frac{2}{n(n+1)}}\left(-\frac{m}{|m|}\right)^m e^{jm\phi}(-j)^{n+1}\\ &\left\{\frac{jm\bar{P}_n^{|m|}(\cos\theta)}{\sin\theta}\hat{\theta} - \frac{\mathrm{d}\bar{P}_n^{|m|}(\cos\theta)}{\mathrm{d}\theta}\hat{\phi}\right\}\end{aligned} \tag{18}$$

$$\begin{aligned}\boldsymbol{K}_{2mn}(\theta,\phi) = &\sqrt{\frac{2}{n(n+1)}}\left(-\frac{m}{|m|}\right)^m e^{jm\phi}(-j)^{n}\\ &\left\{\frac{\mathrm{d}\bar{P}_n^{|m|}(\cos\theta)}{\mathrm{d}\theta}\hat{\theta} + \frac{jm\bar{P}_n^{|m|}(\cos\theta)}{\sin\theta}\hat{\phi}\right\}\end{aligned} \tag{19}$$

B. Rotation and Translation of Spherical Vector Waves

The transformation of the spherical waves in the probe coordinate featured by $\bar{\boldsymbol{x}}^p_{\mathrm{prob}}$, $\bar{\boldsymbol{y}}^p_{\mathrm{prob}}$ and $\bar{\boldsymbol{z}}^p_{\mathrm{prob}}$ to that in the global coordinate featured by $\bar{\boldsymbol{x}}_{\mathrm{glob}}$, $\bar{\boldsymbol{y}}_{\mathrm{glob}}$ and $\bar{\boldsymbol{z}}_{\mathrm{glob}}$ can be decomposed into three phases.

1) Rotate the probe coordinate system so that the new z-axis is directed in the $\bar{\boldsymbol{v}}_p$ direction.
In this phase, the rotation of the spherical wave functions can be described by Euler angles $[\phi_0, \theta_0, \chi_0]$ [16]. ϕ_0 and χ_0 are the rotation about z-axis, and θ_0 is the rotation about y-axis. The rotation about z-axis only results in a phase shift of each spherical wave mode, and the rotation about y-axis needs a set of rotation coefficients. The relation between the original spherical wave functions in the probe coordinate and the ones after rotation is given by
$$\begin{aligned}&\boldsymbol{F}^{(c)}_{\sigma\mu\upsilon}(r',\theta',\phi') =\\ &\sum_{\mu_1=-\upsilon}^{\upsilon} e^{j\mu\phi_0} d^{\upsilon}_{\mu_1\mu}(\theta_0)\, e^{j\mu_1\chi_0}\boldsymbol{F}^{(c)}_{\sigma\mu_1\upsilon}(r'',\theta'',\phi'')\end{aligned} \tag{20}$$
where the rotation coefficient $d^{\upsilon}_{\mu_1\mu}(\theta_0)$ is a real function of θ_0
$$\begin{aligned}d^{\upsilon}_{\mu_1\mu}(\theta_0) = &\sqrt{\frac{(\upsilon+\mu_1)!\,(\upsilon-\mu_1)!}{(\upsilon+\mu)!\,(\upsilon-\mu)!}}\\ &\left(\cos\frac{\theta_0}{2}\right)^{\mu_1+\mu}\left(\sin\frac{\theta_0}{2}\right)^{\mu_1-\mu} P^{(\mu_1-\mu,\mu_1+\mu)}_{\upsilon-\mu_1}(\cos\theta_0)\end{aligned} \tag{21}$$
and $P^{(\alpha,\beta)}_n$ is the Jacobi polynomial.
2) Translate the origin a distance $\|\bar{\boldsymbol{v}}_p\|$ along the $\bar{\boldsymbol{v}}_p$ direction.
In this phase, the translation of the spherical wave functions is given by
$$\begin{aligned}\boldsymbol{F}^{(c)}_{\sigma\mu_1\upsilon}(r'',\theta'',\phi'') = &\sum_{s=1}^{2}\sum_{n=|\mu_1|,n\neq 0}^{\infty}\\ &C^{\sigma\upsilon(c)}_{s\mu_1 n}(k\|\bar{\boldsymbol{v}}_p\|)\,\boldsymbol{F}^{(1)}_{s\mu_1 n}(r''',\theta''',\phi''')\end{aligned} \tag{22}$$
assuming $\|\bar{\boldsymbol{v}}_p\|$ is larger than the probe electric size. C is the translation coefficient
$$\begin{aligned}C^{\sigma\upsilon(c)}_{s\mu_1 n}(kA) = &\frac{1}{2}\sqrt{\frac{(2n+1)(2\upsilon+1)}{n(n+1)\upsilon(\upsilon+1)}}\\ &\sqrt{\frac{(n+\mu_1)!\,(\upsilon-\mu_1)!}{(n-\mu_1)!\,(\upsilon+\mu_1)!}}(-1)^{\mu_1} j^{\upsilon-n}\sum_{p=|\upsilon-n|}^{n+\upsilon}\\ &\Big[j^{-p}\left(\delta_{\sigma s}\left\{n(n+1)+\upsilon(\upsilon+1)-p(p+1)\right\}\right.\\ &\left.+\delta_{3-\sigma,s}\left\{2j\mu_1 kA\right\}\right)(2p+1)\sqrt{\frac{(\upsilon+\mu_1)!\,(n-\mu_1)!}{(\upsilon-\mu_1)!\,(n+\mu_1)!}}\\ &\begin{pmatrix}\upsilon & n & p\\ 0 & 0 & 0\end{pmatrix}\begin{pmatrix}\upsilon & n & p\\ \mu_1 & -\mu_1 & 0\end{pmatrix} z^{(c)}_p(kA)\Big]\end{aligned} \tag{23}$$
where $\begin{pmatrix}\upsilon & n & p\\ 0 & 0 & 0\end{pmatrix}$ is the $3-j$ symbols, and $z^{(c)}_p(kA)$ is the spherical function.
3) Make a final rotation to align the coordinate system with the global coordinate system.

In this phase, the rotation of the spherical wave functions is described by Euler angles $[\phi_0', \theta_0', \chi_0']$, and is given by

$$\boldsymbol{F}_{s\mu_1 n}^{(1)}\left(r''', \theta''', \phi'''\right) = \sum_{m=-n}^{n} e^{j\mu_1 \phi_0'} d_{m\mu_1}^{n}\left(\theta_0'\right) e^{jm\chi_0'} \boldsymbol{F}_{smn}^{(1)}\left(r, \theta, \phi\right) \tag{24}$$

Combining (20), (22), and (24), the spherical wave functions in the probe coordinate is thus describe by the spherical wave functions in the global coordinate of the test zone.

REFERENCES

[1] CTIA Certification, "Test Plan for Wireless Device Over-the-Air Performance," V 3.7.1, Feb. 2018.

[2] P. Kyosti, T. Jamsa, J.P. Nuutinen, "Channel modeling for multiprobe over-the-air MIMO Testing," *Int. J. Antennas Propag.,* vol. 2012, no. 615954, Mar. 2012.

[3] W. Fan, I. Carton, P. Kyosti, and G.F. Pedersen, "Emulating ray-tracing channels in multiprobe anechoic chamber setups for virtual drive testing," *IEEE Trans. Antennas Propag.*, vol. 64, no. 2, Feb. 2016.

[4] A. Khatun, V.M. Kolmonen, V. Hovinen, D. Parveg, M. Berg, K. Haneda, K.I. Nikoskinen, E.T. Salonen, "Experimental verification of a plane-wave field synthesis technique for MIMO OTA antenna testing," *IEEE Trans. Antennas Propag.*, vol. 64, no. 7, Jul. 2016.

[5] J. Toivanen, T. Laitinen, V. Kolmonen, and P. Vainikainen, "Reproduction of arbitrary multipath environment in laboratory conditions," *IEEE Transaction on Instrumentation and Measurement,* vol. 60, no. 1, pp. 275-281, 2011.

[6] W. Fan, X. Carreno, F. Sun, J. Nielsen, M.B. Knudsen, and G.F. Pedersen, "Emulating spatial characteristics of MIMO channels for OTA testing," *IEEE Trans. Antennas Propag.,* vol. 61, no. 8, pp. 4306-4314, 2013.

[7] P.S. Kildal, X. Chen, C. Orlenius, M. Franzen, C.S.L. Patane, "Characterization of reverberation chambers for OTA measurements of wireless devices: physical formulations of channel matrix and new uncertainty formula," *IEEE Trans. Antennas Propag.*, vol. 60, no. 8, Aug. 2012.

[8] X. Chen, "Throughput modeling and measurement in an isotropic scattering reverberation chamber," *IEEE Trans. Antennas Propag.,* vol. 62, no. 4, pp. 2130-2139, 2014.

[9] J. Karedal, F. Tufvesson, N. Czink, A. Paier, C. Dumard, T. Zemen, C.F. Mecklenbrauker, A.F. Molisch, "A geometry-based stochastic MIMO model for vehicle-to-vehicle communications," *IEEE Transactions on Wireless Communications,* vol. 8, no. 7, pp. 3646-3657, Jul. 2009.

[10] W. Fan, X. Carreo, J. Nielsen, J.S. Ashta, G.F. Pedersen, M.B. Knudsen, "Verification of emulated channels in multi-probe based MIMO OTA testing setup," in *Proc. 7th Eur. Conf. Antenna Propag.,* pp. 97-101, Gothenburg, Sweden, Apr. 2013.

[11] P. Kyosti, L. Hentila, "Criteria for physical dimensions of MIMO OTA multi-probe test setup," in *Proc. 6th Eur. Conf. Antenna Propag.,* Prague, Czech Republic, Jun. 2012.

[12] T. Laitinen, P. Kyosti, "On appropriate probe configurations for practical MIMO over-the-air testing of wireless devices," *Proc. 6th Eur. Conf. Antenna Propag.,*, Prague, Czech Republic, Jun. 2012.

[13] Y. Ji, W. Fan, G.F. Pedersen, X. Wu, "On channel emulation methods in multi-probe anechoic chamber setups for over-the-air testing," *IEEE Trans. Vehicular Technology*, vol. 67, no. 8, Aug. 2018.

[14] B. Derat, "5G antenna characterization in the far-field — how close can far-field be," *2018 IEEE International Symposium on Electromagnetic Compatibility and 2018 IEEE Asia-Pacific Symposium on Electromagnetic Compatibility (EMC/APEMC)*, Singapore, May 2018.

[15] A. Khatun, T. Laitinen, V.M. Kolmonen, P. Vainikainen, "Dependence of error level on the number of probes in over-the-air multiprobe test systems," *International Journal of Antennas and Propagation*, vol. 2012, no. 624174, Mar. 2012.

[16] J.E. Hansen, *Spherical Near-Field Antenna Measurements.* London, U.K.: Peregrinus, 1988.

[17] Y. Miao, K. Haneda, M. Kim, J. Takada, "Antenna de-embedding of radio propagation channel with truncated modes in the spherical vector wave domain," *IEEE Trans. Antennas Propag.*, vol. 63, no. 9, pp. 4100-4110, Sep. 2015.

[18] J. Naganawa, J. Takada, T. Aoyagi, M. Kim, "Antenna deembedding in WBAN channel modeling using spherical wave functions," *IEEE Trans. Antennas Propag.*, vol. 65, no. 3, pp. 1289-1300, Jan. 2017.

[19] P. Kyosti, A. Khatun, "Probe configurations for 3D MIMO over-the-air testing," *7th European Conference on Antennas and Propagation (EuCAP)*, Gothenburg, Sweden, Apr. 2013.

[20] Y. Miao, J.I. Takada, "Pattern reconstruction for deviated AUT in spherical measurement by using spherical waves," *IEICE Transactions on Communications,* vol. E97-B, no. 1, pp. 105-113, Jan. 2014.

[21] M. Sonkki, D. Sanchez-Escuderos, V. Hovinen, E.T. Salonen, and M. Ferrando-Bataller, "Wideband dual-polarized cross-shaped Vivaldi antennas," *IEEE Trans. Antennas Propag.*, vol. 63, no. 6, Jun. 2015.

Yang Miao received the M. Sc. and the Ph.D. degrees from the antenna and radio propagation lab, Department of International Development Engineering, Tokyo Institute of Technology, Japan, in 2012 and 2015, respectively. From October 2010 to September 2015, she was a Research Assistant with Takada Lab, the Mobile Communications Research Group (MCRG), Tokyo Institute of Technology. From October 2015 to January 2018, she was a Postdoctoral Researcher with Institute of Information and Communication Technologies, Electronics and Applied Mathematics (ICTEAM), Université Catholique de Louvain, and with the IMEC/WAVES (Wireless, Acoustics, Environment and Expert Systems) lab, Ghent University, Belgium. She stayed with Jaguar Radio Wave Corporation, Shenzhen, China, from October 2017 to March 2018, as a part-time Senior Antenna Engineer. From April 2018, she became a Research Assistant Professor in Southern University of Science and Technology, Shenzhen, China.

Her scientific work is focused on the interaction between antenna arrays and physical radio propagation environment. Her studies dealt with spherical antenna measurement, array radiation pattern reconstruction in spatial and frequency domains, indoor radio channel measurement, antenna-channel interaction, antenna de-embedding and channel modeling in both plane wave and spherical vector wave domains, diffuse scattering correlation for radio propagation prediction, reverberation channel prediction using hybrid methods of ray tracing and propagation graph, human detection and positioning using indoor radio channel properties, over-the-air testing emulation algorithm in multi-probe anechoic chamber, and unmanned aerial vehicle air-to-ground radio propagation.

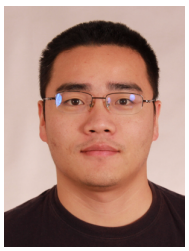

Wei Fan received his Bachelor of Engineering degree from Harbin Institute of technology, China in 2009, Master's double degree with highest honours from Politecnico di Torino, Italy and Grenoble Institute of Technology, France in 2011, and Ph.D. degree from Aalborg University, Denmark in 2014. From February 2011 to August 2011, he was with Intel Mobile Communications, Denmark as a research intern. He conducted a three-month internship at Anite telecoms oy (now Keysight Technologies), Finland in 2014. He is currently an associate professor at Aalborg University. His main areas of research are over the air testing of multiple antenna systems, radio channel sounding, parameter estimation, modeling and emulation.

Junichi Takada received Doctor of Engineering in electrical and electronic engineering from Tokyo Institute of Technology (Tokyo Tech) in 1992. After serving as a Research Associate at Chiba University in 1992-1994, and as an Associate Professor at Tokyo Tech in 1994-2006, he has been a Professor at Tokyo Tech since 2006. Currently he is serving as the vice chair of the Department of Transdisciplinary Science and Engineering, School of Environment and Society, Tokyo Tech. From 2003 to 2007, he was also a Researcher at the National Institute of Information and Communication Technology, Japan. His current research interests include radio-wave propagation and channel modeling for mobile and short range wireless systems, applied measurement using radio wave, and ICT applications for international development. He is a fellow of Information and Communication Engineering (IEICE), Japan, a senior member of IEEE, and a member of Japan Society for International Development.

Ruisi He (S'11-M'13-SM'17) received the B.E. and Ph.D. degrees from Beijing Jiaotong University (BJTU), Beijing, China, in 2009 and 2015, respectively. Since 2015, Dr. He has been with the State Key Laboratory of Rail Traffic Control and Safety, BJTU, where he has been a Full Professor since 2019. Dr. He has been a Visiting Scholar in Georgia Institute of Technology, USA, University of Southern California, USA, and Université Catholique de Louvain, Belgium. His research interests include measurement and modeling of wireless channels, machine learning and clustering analysis in communications, vehicular and high-speed railway communications, 5G massive MIMO and high frequency communication techniques. He has authored/co-authored 3 books, 3 book chapters, more than 100 journal and conference papers, as well as several patents.

Dr. He is an Editor of the IEEE TRANSACTIONS ON WIRELESS COMMUNICATIONS, the IEEE ANTENNAS AND PROPAGATION MAGAZINE, and the IEEE COMMUNICATIONS LETTERS. He serves as the Early Career Representative (ECR) of Commission C, International Union of Radio Science (URSI). He has been a Technical Program Committee (TPC) chair and member for many conferences and workshops. He received 2017-2019 Young Talent Sponsorship Program of China Association for Science and Technology, the Second Prize of the Natural Science Award for Scientific Research Achievements of the Ministry of Education in China in 2016, the Best Ph.D. Thesis Award of Chinese Institute of Electronics in 2016, the URSI Young Scientist Award in 2015, and five Best Paper Awards in conferences. He is a member of the COST.

Xuefeng Yin received his Bachelor degree in optoelectronics engineering from Huazhong University of Science and Technology, Wuhan, China, in 1995, and the M.S. degree in digital communications and the Ph.D. degree in wireless communications from Aalborg University, Denmark, in 2002 and 2006, respectively. From 2006 to 2008, he worked as an Assistant Professor in Aalborg University. In 2008, he joined the college of electronics and information engineering, Tongji University, Shanghai, China, where he has been a Full Professor and Vice Dean since 2016. He has published more than 120 technical papers and co-authored the book Propagation channel characterization, parameter estimation and modeling for wireless communications John Wiley and Sons IEEE Edition in 2016. His current research interests include high-resolution parameter estimation for propagation channels, measurement-based channel characterization and stochastic channel modeling, channel simulation based on random propagation graph models, radar signal processing, and positioning.

Mi Yang received the B.S. degree and the M.S. degree in Electronic and Communication Engineering from Beijing Jiaotong University, in 2014 and 2016, respectively. He has been pursuing the Ph.D. degree from the State Key Laboratory of Rail Traffic Control and Safety at Beijing Jiaotong University, China. His research interests are focused on radio propagation models, vehicle-to-vehicle communications and software defined radio.

José Rodríguez-Piñeiro received the B.Sc. on Telecommunications and the M.Sc. Degree in Signal Processing Applications for Communications from the University of Vigo (Pontevedra, Spain), in 2009 and 2011, respectively. Between June 2008 and July 2011, he was a researcher at the Department of Signal and Communications, University of Vigo (Pontevedra, Spain). From October 2011, he was a researcher at the Group of Electronics Technology and Communications of the University of A Corua (UDC), obtaining his Ph.D. degree with the distinction "Doctor with European Mention" in 2016. After obtaining his Ph.D. degree, he continued working as a Postdoctoral researcher at the same group until July 2017. On August 2017, he joined the College of Electronics and Information Engineering, Tongji University (P.R. China). From November 2012, he also collaborates with the Department of Power and Control Systems, National University of Asuncin (Paraguay) in both teaching and research. He is the coauthor of more than 30 papers in peer-reviewed international journals and conferences. He is also a member of the research team in more than 20 research projects funded by public organizations and private companies. He was awarded with 6 predoctoral, postdoctoral and research stay grants. His research interests include experimental evaluation of digital mobile communications, especially for high mobility environments, including terrestrial and aerial vehicular scenarios.

Andrés Alayón Glazunov (SM'11) was born in Havana, Cuba, in 1969. He received the M.Sc. degree in physical engineering from Peter the Great St. Petersburg Polytechnic University (Polytech), Saint Petersburg, Russia, in 1994, the Ph.D. degree in electrical engineering from Lund University, Lund, Sweden, in 2009, and the Docent (Habilitation) degree in antenna systems from the Chalmers University of Technology, Gothenburg, Sweden, in 2017.

From 1996 to 2005, he held various research and specialist positions at telecom industry, e.g., Ericsson Research, Telia Research, and TeliaSonera, all in Stockholm, Sweden. From 2001 to 2005, he was the Swedish delegate to the European Cost Action 273 and was active in the Handset Antenna Work Group. From 2009 to 2010, he was a Marie Curie Senior Research Fellow with the Centre for Wireless Network Design, University of Bedfordshire, Luton, U.K. From 2010 to 2014, he held a postdoctoral position with the Electromagnetic Engineering Laboratory, KTH-Royal Institute of Technology, Stockholm. From 2014 to 2018, he was an Assistant Professor with the Chalmers University of Technology. Dr. Glazunov has contributed to and initiated various European Research Projects, e.g., currently, the is3DMIMO, the WAVECOMBE, and the Build-Wise Projects under the auspices of the H2020 European Research and Innovation Program. He has also contributed to the international 3GPP and the ITU standardization bodies. He has been one of the pioneers in establishing over-the-air measurement techniques.

Currently, Dr. Glazunov is an Associate Professor with the Department of Electrical Engineering, University of Twente, Enschede, The Netherlands, and also affiliated with the Chalmers University of Technology. He is leading the Radio, Propagation and Antenna Systems Research Group, University of Twente, while at Chalmers, he is leading the over-the-air (OTA) characterization of antenna systems research area. He is currently the Dutch delegate to the IRACON Cost Action. He has authored more than 100 scientific and technical publications. He has co-authored and co-edited the text book LTE-Advanced and Next Generation Wireless Networks Channel Modeling and Propagation (Wiley, 2012). His current research interests include, but are not limited to, MIMO antenna systems, electromagnetic theory, fundamental limitations on antennachannel interactions, radio propagation channel measurements, modeling and simulations, and the OTA characterization of antenna systems and wireless devices.

Wei Wang (M'09) received the Bachelor degree in the field of communications engineering from University of Wuhan, China, in 2003, the Master degree from University of Kiel, Germany, in 2006 and the Doctoral degree with summa cum laude from University of Erlangen-Nuremberg, Germany, in 2014.

From 2007 to 2018, he has worked as a scientific staff member at the Institute of Communications and Navigation of German Aerospace Center (DLR), Oberpfaffenhofen, Germany. Now he is a professor with the School of Information Engineering at Chang'an University, China. His research interests include time variant parameter estimation, channel modeling for localization and navigation, channel measurements, terrestrial radio based positioning/navigation and related topics. He received the best presentation paper award in ION GNSS 2012, best paper award in EUCAP 2018 and in COTA 2018. He is an associate editor in IET Microwave, Antennas and Propagation, and served as TPC member for ICC and VTC conference and workshops

Yi Gong (S'99, M'03, SM'07) received his Ph.D. degree in electrical engineering from The Hong Kong University of Science and Technology, Hong Kong, in 2002. He was with the Hong Kong Applied Science and Technology Research Institute, Hong Kong, and Nanyang Technological University, Singapore. He is currently a Professor at the Southern University of Science and Technology, Shenzhen, China. From 2006 to 2018, he served on the Editorial Board of the IEEE Transactions on Wireless Communications and the IEEE Transactions on Vehicular Technology. His research interests include cellular networks, mobile computing, channel modeling, and signal processing for wireless communications and related applications.